



HAL
open science

Anoctamin 5 Knockout Mouse Model Recapitulates LGMD2L Muscle Pathology and Offers Insight Into in vivo Functional Deficits

Girija Thiruvengadam, Sen Chandra Sreetama, Karine Charton, Marshall Hogarth, James S Novak, Laurence Suel-Petat, Goutam Chandra, Bruno Allard, Isabelle Richard, Jyoti K Jaiswal

► To cite this version:

Girija Thiruvengadam, Sen Chandra Sreetama, Karine Charton, Marshall Hogarth, James S Novak, et al.. Anoctamin 5 Knockout Mouse Model Recapitulates LGMD2L Muscle Pathology and Offers Insight Into in vivo Functional Deficits. *Journal of Neuromuscular Diseases*, 2021, 8 (s2), pp.S243-S255. 10.3233/JND-210720 . hal-03433538v2

HAL Id: hal-03433538

<https://hal-univ-evry.archives-ouvertes.fr/hal-03433538v2>

Submitted on 29 Nov 2021

HAL is a multi-disciplinary open access archive for the deposit and dissemination of scientific research documents, whether they are published or not. The documents may come from teaching and research institutions in France or abroad, or from public or private research centers.

L'archive ouverte pluridisciplinaire **HAL**, est destinée au dépôt et à la diffusion de documents scientifiques de niveau recherche, publiés ou non, émanant des établissements d'enseignement et de recherche français ou étrangers, des laboratoires publics ou privés.

Anoctamin 5 Knockout Mouse Model Recapitulates LGMD2L Muscle Pathology and Offers Insight Into *in vivo* Functional Deficits

Girija Thiruvengadam^{a,1}, Sen Chandra Sreetama^{a,1}, Karine Charton^b, Marshall Hogarth^a,
James S. Novak^{a,d}, Laurence Suel-Petat^b, Goutam Chandra^a, Bruno Allard^c,
Isabelle Richard^{b,*} and Jyoti K. Jaiswal^{a,d,*}

^aCenter of Genetic Medicine Research, Children's National Health System, MW Washington, DC

^bGénéthon INSERM, U951, INTEGRARE Research Unit, University Paris-Saclay, Evry, France

^cUniversité Lyon, Université Claude Bernard Lyon 1, Institut NeuroMyoGene, Centre National de la Recherche Scientifique, Institut National de la Santé et de la Recherche Médicale, Lyon, France

^dDepartment of Genomics and Precision Medicine, George Washington University School of Medicine and Health Sciences, Washington DC

Abstract. Mutations in the Anoctamin 5 (*Ano5*) gene that result in the lack of expression or function of ANO5 protein, cause Limb Girdle Muscular Dystrophy (LGMD) 2L/R12, and Miyoshi Muscular Dystrophy (MMD3). However, the dystrophic phenotype observed in patient muscles is not uniformly recapitulated by ANO5 knockout in animal models of LGMD2L. Here we describe the generation of a mouse model of LGMD2L generated by targeted out-of-frame deletion of the *Ano5* gene. This model shows progressive muscle loss, increased muscle weakness, and persistent bouts of myofiber regeneration without chronic muscle inflammation, which recapitulates the mild to moderate skeletal muscle dystrophy reported in the LGMD2L patients. We show that these features of ANO5 deficient muscle are not associated with a change in the calcium-activated sarcolemmal chloride channel activity or compromised *in vivo* regenerative myogenesis. Use of this mouse model allows conducting *in vivo* investigations into the functional role of ANO5 in muscle health and for preclinical therapeutic development for LGMD2L.

INTRODUCTION

Muscular dystrophies are a diverse group of inherited diseases that result in progressive loss of muscle structure and function, that leads to weakness and wasting of skeletal muscle. Among these, the Limb-girdle muscular dystrophies (LGMD) represent a group of myopathies where severely affected muscles include the hip and shoulder girdles, with subsequent involvement of other limb muscles. LGMD

¹Equal Contribution.

*Correspondence to: Isabelle Richard, Généthon INSERM, U951, INTEGRARE Research Unit, University Paris-Saclay, Evry, France. Tel.: +33.1.69.47.29.38; E-mail: RICHARD@Genethon.fr.; Jyoti K. Jaiswal, Department of Genomics and Precision Medicine, George Washington University School of Medicine and Health Sciences, Washington DC Tel.: +1.202.476.6456; E-mail: jkjaishwal@cnmc.org.

33 results in progressive muscle weakness from early
34 childhood to late adulthood. Over two dozen genes
35 responsible for LGMD have been identified, which
36 lead to either recessive or dominant inheritance [1,
37 2]. LGMD2L/ LGMDR12 is a recessive disorder
38 with a prevalence of 0.2–2 patients / 100,000 that
39 is amongst the 5 most common LGMDs [3–5]. It
40 is caused by mutations in the gene that encodes
41 the Anoctamin 5 (ANO5) or the Transmembrane16E
42 (TMEM16E) protein [6–9]. ANO5/TMEM16E pro-
43 tein belongs to a family of 10 related transmembrane
44 proteins that function either as calcium-activated ion
45 channels, lipid scramblases, or both [10, 11]. Among
46 these, ANO1 (TMEM16A) and ANO2 (TMEM16B)
47 encode calcium-activated chloride channels, while
48 ANO6 (TEME16F) and ANO10 (TMEM16K) are
49 phospholipid scramblases (PLS) [10–22]. ANO5 is
50 the only member of this family that is associated
51 with muscular dystrophy. This gene is expressed in
52 bones, skeletal muscles, testes, and cardiac mus-
53 cles [23–25]. Unlike the recessive *Ano5* mutations,
54 dominant mutations in *Ano5* lead to the bone disor-
55 der, gnathodiaphyseal dysplasia 1 (GDD1) [25, 26].
56 While GDD1 is characterized by bone fragility and
57 jawbone lesions, LGMD2L/R12 is characterized by
58 increased serum level of muscle enzyme, myofiber
59 damage, sporadic rhabdomyolysis, exercise-induced
60 myalgia, proximal limb muscle pain and weakness,
61 and difficulty walking and standing on toes [6, 8].
62 Many of these clinical features are shared with other
63 muscular dystrophies such as LGMD2B/R2, where
64 mutations reduce or prevent expression of the mem-
65 brane protein dysferlin, leading to increased myofiber
66 death and muscle degeneration [27–29].

67 Endogenous ANO5 protein localizes to the Sarco/
68 Endoplasmic Reticulum (SER) membrane, but exo-
69 genously expressed ANO5 is detected at the plasma
70 membrane where it exhibits calcium-activated scr-
71 amblase as well as ion channel activity [21, 25,
72 30–34]. We recently identified the requirement of
73 endogenously expressed ANO5 for calcium-act-
74 ivated calcium uptake by the SER during cellular cal-
75 cium overload [24, 35]. The ion channel and lipid
76 scramblase activities of ANO5 have been implicated
77 in sarcolemmal repair, myoblast fusion during muscle
78 regeneration, and mouse sperm motility [24, 34–39].
79 Further, biochemical studies of ANO5 and targeted
80 GDD1 and LGMD2L patient mutations suggest that
81 while the GDD1 associated mutations result in gain of
82 ANO5 function, LGMD2L/R12 mutations are asso-
83 ciated with the loss of ANO5 activity [30]. This
84 view is supported by the observation that patient cells

85 lacking detectable ANO5 protein exhibit poor mem-
86 brane repair [24, 35], indicating that *Ano5* knockout
87 would be a suitable animal model for LGMD2L/R12.

88 Knockout animal models targeting different reg-
89 ions of *Ano5* gene have been generated previously.
90 While deletion of the first two exons of *Ano5* results
91 in no detectable muscle deficits [23, 39], *Ano5* dis-
92 ruption in mouse by insertional deletion of exons 8–9
93 results in notable muscle pathology [37], and deletion
94 of exons 11–12 leads to bone weakness [40]. Dele-
95 tion of exons 12–13, with consequent disruption of
96 the *Ano5* reading frame in rabbits faithfully recapitu-
97 lates the dystrophic muscle features [41]. With these
98 diverse outcomes identified from *Ano5* knockout ani-
99 mal models, here we describe a ANO5 knockout
100 mouse model to investigate the ANO5 function in
101 muscular dystrophy. Our works build on two previ-
102 ous findings – symptomatic animal models involve
103 disruption of *Ano5* gene in the region spanning exons
104 8–12, and cells lacking ANO5 protein exhibit ion
105 homeostasis and sarcolemmal repair deficit [30, 35].
106 With ANO5 function linked to muscle cell mem-
107 brane repair, *in vitro* myoblast fusion, and plasma
108 membrane ion channel activity [24, 30–39], we have
109 examined these activities *in vivo* and assessed their
110 impact on muscle pathology in our model. Our find-
111 ings establish a new mouse model of LGMD2L and
112 the characterization we present here offers insights
113 into the *in vivo* relevance of ANO5 function for mus-
114 cle pathology in LGMD2L.

115 METHODS

116 *Animals and knockout mouse generation*

117 All animal procedures were conducted in accorda-
118 nce with guidelines for the care and use of labora-
119 tory animals and were approved by the Children’s
120 National Research Institute Animal Care and Use
121 Committee (#00030709), the local animal ethics
122 committee of University Lyon 1 and Ethical Com-
123 mittee for Animal Experimentation C2EA-51 of Evry
124 (#APAFIS#01304.01). C57BL/6J (WT) mice were
125 obtained from the Jackson Laboratory (Bar Harbor,
126 ME) and maintained in our animal facility for the
127 purpose of this study. All animals were maintained
128 in an individually vented cage system under a con-
129 trolled 12 h light/dark cycle with free access to food
130 and water and animals of both genders were used for
131 experiments.

132 Construction of the targeting vector and genera-
133 tion of the ANO5 knockout mouse was performed

by Genoway (Lyon). A bacterial artificial chromosome (BAC) library was screened using *Ano5* primers allowing the identification of 3 clones covering the genomic region around exons 11 to 13 of the *Ano5* gene. These BAC were used to construct the targeting vector, which was electroporated into ES cells. After selection and analysis of the homologous recombination events, two positive ES clones were selected and then injected into C57BL/6J blastocysts that were reimplanted into foster mothers to generate chimeric mice. Five highly chimeric males were obtained and bred first with the deleter mice, constitutively expressing the Flp recombinase for deletion of the neomycin selection cassette. Resulting animals were mated with mice transgenic for CMV-CRE, which permits the excision of the floxed *Ano5* segment. The Cre transgene was segregated by a first cross on C57BL/6 background and the resulting heterozygous mice were backcrossed for 10 generations on the C57BL/6 and then interbred. For genotyping, genomic DNA from mouse tail was extracted and amplified using KAPA2G Fast Hot-Start Genotyping Mix, (Sigma, St. Louis, MO, USA) with the following: 49683cre-IRII.F: attcctgagaata tgtgtaattgtggcagc 49698flp-IRII.R: 5'-ccctagaactaca taatcttggtgtggtgtag -3'. A PCR fragment of 2,68 kb is generated for the WT allele and of 890 bp for the mutant allele.

In vivo muscle injury, bromodeoxyuridine (BrdU) labelling, and immunostaining

Muscles were injured by local injection of notexin in 10-month-old animals under isoflurane anaesthesia (42). Following removal of fur from the anterior hindlimb, 40 μ l notexin (5 μ g/ml, Latoxan, #L8104) was delivered by intramuscular injection into the *tibialis anterior* (TA) using a 0.3 ml ultrafine insulin syringe (BD Biosciences, #324906). Immediately prior to injection, the needle was dipped in green tattoo dye (Harvard Apparatus, #72-9384) to mark the needle track. For the first 7 days post injury, BrdU (Sigma-Aldrich, B9285) was administered ad libitum in sterile drinking water at a concentration of 0.8 mg/ml. Animals were euthanized either 7- or 14-days post-injury, and tissues were harvested for analysis [43, 44].

Skeletal muscles were dissected out and frozen in isopentane cooled in liquid nitrogen. Transverse cryosections (8- μ m thickness) were prepared from frozen muscles and were processed for hematoxylin and eosin (H&E) and Laminin staining. Frozen

sections were cut and fixed in ice-cold acetone for 10 min, followed by incubation in 2N HCl at 37°C for 30 min, and then briefly neutralized with 0.15M sodium tetraborate (Sigma-Aldrich, MO). Following this, sections were blocked for 1 h in phosphate-buffered saline (PBS) supplemented with 20% goat serum (GeneTex, CA), 0.1% tween-20 (Sigma-Aldrich, MO), and 10 mg/ml BSA (Sigma-Aldrich, MO). Primary antibodies against BrdU (B35138, 1 : 100, Life Technologies, CA) and laminin (L9393, 1 : 400, Sigma-Aldrich, MO) were incubated overnight at 4°C. Sections were then washed and probed with the appropriate Alexa Fluor secondary antibody (Life Technologies, MA) at a dilution of 1 : 500 for 1 h at room temperature. Prior to mounting, nuclei were counterstained with propidium iodide (P4170, 2.5 μ g/ml, Sigma-Aldrich, MO). Digital images were captured with a VS120 virtual slide microscope, and images were processed and quantified using CellSens and ImageJ software.

Muscle force measurements

Forelimb and hindlimb grip-strength measurement (GSM) were carried out using a grip strength meter (Columbus Instruments, Columbus, OH, USA) as previously described [45]. The animals were acclimatized for 3 days before actual data collection. The forelimb and hindlimb grip-strength data were then collected over 5 consecutive days. Data were represented as averaged grip strength/kg body weight over 5 days.

To measure *in vivo* torque production of the anterior crural muscles (TA, *extensor digitorum longus* (EDL), *peroneus tertius*, and *extensor hallucis longus*), mice were anesthetized with 1.5% isoflurane-mixed O₂ and hair was removed from the lower hind limbs, while the foot was attached to the dual-mode lever and maintained at a 90° angle for isometric torque assessment (Aurora Scientific, Aurora, Canada). Isometric muscle contractions were stimulated at 1.0–2.0 mA using Pt-Ir needle electrodes inserted percutaneously adjacent to the peroneal nerve. Peak isometric torque was measured in response to tetanic stimulations at 20, 40, 60, 80, 100, 120, 140, 160, 180, and 200 Hz, providing a 60s rest period between stimuli. The rate of rise in torque was modeled using the exponential equation $T = C(1 - e^{-Df})$, where T = torque produced at the given frequency (f), C = maximal torque, and D = the rate of rise in torque [46]. Here, we tested 10-month-old, male WT and ANO5^{-/-} mice ($n = 5$).

Myofiber isolation and electrophysiology

Mice were euthanized by cervical dislocation followed by removal of *flexor digitorum brevis* (FDB) muscles. Single fibers were isolated by a 50-minute enzymatic treatment at 37° C using a Tyrode solution containing 2 mg/mL collagenase type I (Sigma). Fibers were voltage-clamped using the silicone clamp technique as previously described [47]. Briefly, a major part of a single fiber was electrically insulated with silicone grease and a micropipette was inserted into the fiber through the silicone layer to voltage clamp the portion of the fiber free of grease (50 to 150 μm length) using a patch-clamp amplifier (Bio-Logic RK-400, Claix, France) in whole-cell configuration. Analog compensation was systematically used to decrease the effective series resistance. The tip of the micropipette was then crushed into the dish bottom to allow intracellular dialysis of the fiber with the intra-pipette solution. Cell capacitance was determined by integration of a current trace obtained with a 10-mV hyperpolarizing pulse from the holding potential and was used to calculate the density of currents (A/F). Currents were acquired at a sampling frequency of 10 kHz. Data are given as means ± S.E.M.

The external solution contained (in mM) 140 TEA-MeSO₃ (9 mM Cl⁻ containing solution) or 140 TEA-Cl (149 mM Cl⁻ containing solution), 2.5 CaCl₂, 2 MgCl₂, 0.002 tetrodotoxin, 1 4-aminopyridine and 10 HEPES adjusted to pH 7.2 with TEA-OH. The internal dialyzed solution contained (in mM) 140 K-glutamate, 2 EGTA, 5 Na₂-ATP, 5 Na₂-phosphocreatine, 5 MgCl₂, 5 glucose and 10 HEPES adjusted to pH 7.2 with K-OH. The 2 mM internal [EGTA] prevented deterioration of the muscle fiber in response to large depolarizing pulses but preserved fiber contraction upon suprathreshold depolarizations. Fibers were dialyzed with the intracellular solution through the micropipette during 10 min prior starting the experiments.

RNA isolation and quantitative RT-PCR

RNA was extracted by the Trizol method from muscles previously sampled and frozen in liquid nitrogen. Residual DNA was removed from the samples using Free DNA kit or Turbo DNA-free Kit (Ambion). One μg of RNA was reverse transcribed using the SuperScript II first strand synthesis kit (Invitrogen) or revertAid H Minus First Strand cDNA Synthesis kit (ThermoFisher) and random hexamers.

Real-time PCR was performed using LightCycler480 29437 (Roche) Taqman Gene Expression or miR Assays (ThermoFisher) or 0.2 μM of each primer and 0.1 μM of the probe according to the protocol Absolute QPCR Rox Mix (ThermoFisher).

Endogenous gene expression was quantified using Taqman Gene Expression Assay: ANO5: Mm00624629_m1; ANO6: Mm00614693_m1; ANO8: Mm01343244_m1, MYMK Mm00481256_m1, CD11b Mm00434455_m1, MYH3 Mm01332463_m1, CD3G Mm00438095_m1, TIMP-1 Mm0131, IL1β Mm00434228_m1, IL6 Mm00446190_m1, PLIN5 Mm00508852_m1, and COL6A3 Mm00711678_m1. The ubiquitous acidic ribosomal phosphoprotein (P0) was used to normalize the data across samples. The primer pairs and Taqman probe used for P0 amplification were: m181PO.F (5'-CTCCAAG CAGATGCAGCAGA-3'), m267PO.R (5'-ACCAT GATGCGCAAGGCCAT-3'), m225PO.P (5'-CCG TGGTGCTGATGGGCAAGAA-3') and each experiment was separately replicated.

Expression of miRNA were performed using TaqMan Assays miRNA: miR-21 (hsa-miR-21-5p) ref: 000397, miR-142 (hsa-miR142-3p) ref: 000464, miR-31 (mmu-miR-31-5p) ref: 000185, miR 1(hsa-miR1-3p) ref: 000385, miR-29a (hsa-miR29a-3p) ref: 002112, and normalized using the expression of U6 (U6 snRNA) ref: 001973. Fold change in RNA expression (Fc) in tissues from ANO5-KO mice was calculated using the traditional 2^{-(ΔΔC_t)} method: Fc = 2^{-(ΔC_t - Avg ΔC_t WT)}, allowing comparison of C_t value with that obtained from tissue of WT animals. Evaluation of consequences at RNA level of the mutation in the model was performed by RT-PCR on muscle extracts with the following primers (Ex6.F : GAAGACGAGAGTTTGAACAA AATCTCAGAAAAACAG, Ex14.R : CAAAGTAC-CATGGGATGCGATGGC). The PCR generated fragments of 1080 bp in WT and 778 bp in ANO5-/-.

Statistical analysis

The statistical analysis was carried out using the GraphPad 8.0 Prism Software, where the data were examined by pairwise testing by Mann-Whitney U test or by Analysis of Variance (ANOVA). Outcome of the statistical test is represented in the figures by way of *p* values as indicated in figure legends. Each plot shows the individual data point with the average representing ~~statistical mean and errors bars~~, unless noted otherwise, ~~indicate standard deviation (SD)~~.

RESULTS

Generation of ANO5 knockout mouse model for LGMD2L

To generate the mouse model of LGMD2L/R12, we synthesized a mouse *Ano5* targeting vector composed of a long homology arm of 5.7 kb and a short arm of 1.9 kb on each side of a region encompassing exons 11–13 flanked by *LoxP* sites. Positive selection by neomycin gene flanking by *FRT* sequences was also added in the vector. Through homologous recombination using this vector we disrupted the predicted transmembrane domain of the mouse ANO5 protein, by out of frame deletion of exons 10 to 12 (Fig. 1A). In the resulting chimeric animals, the *neo* gene and rest of the insertional cassette was excised by crossing with *Flp* and *CRE* recombinase under the control of the ubiquitous *CMV* promoter. *Ano5*

deficient mice were generated by a targeted 1793 bp deletion in the *Ano5* genomic loci, which was confirmed by PCR genotyping (Fig. 1B). Absence of the 301 bp spanning exons 10–12 in the resulting mRNA transcript was confirmed by RT-PCR analysis and RNA sequencing (Fig. 1C–E). Congenic ANO5 deficient mice were backcrossed onto the C57Bl/6 genetic background for 10 generations with subsequent interbreeding. Homozygous *Ano5*^{-/-} mice are viable and fertile with no gross abnormalities or increased mortality up to 1 year of age.

To assess the consequences of the targeted knockout of *Ano5*, we quantified *Ano5* transcript levels in skeletal muscle by quantitative RT-PCR (qRT-PCR) analysis. This revealed low-levels of *Ano5* transcript (< 10 % of WT level) in various muscles (Fig. 1F). In view of the role of ANO5 protein in regulating plasma membrane (PM) and Sarco/Endoplasmic Reticulum (SER) function [24, 48, 49], we used qRT-PCR

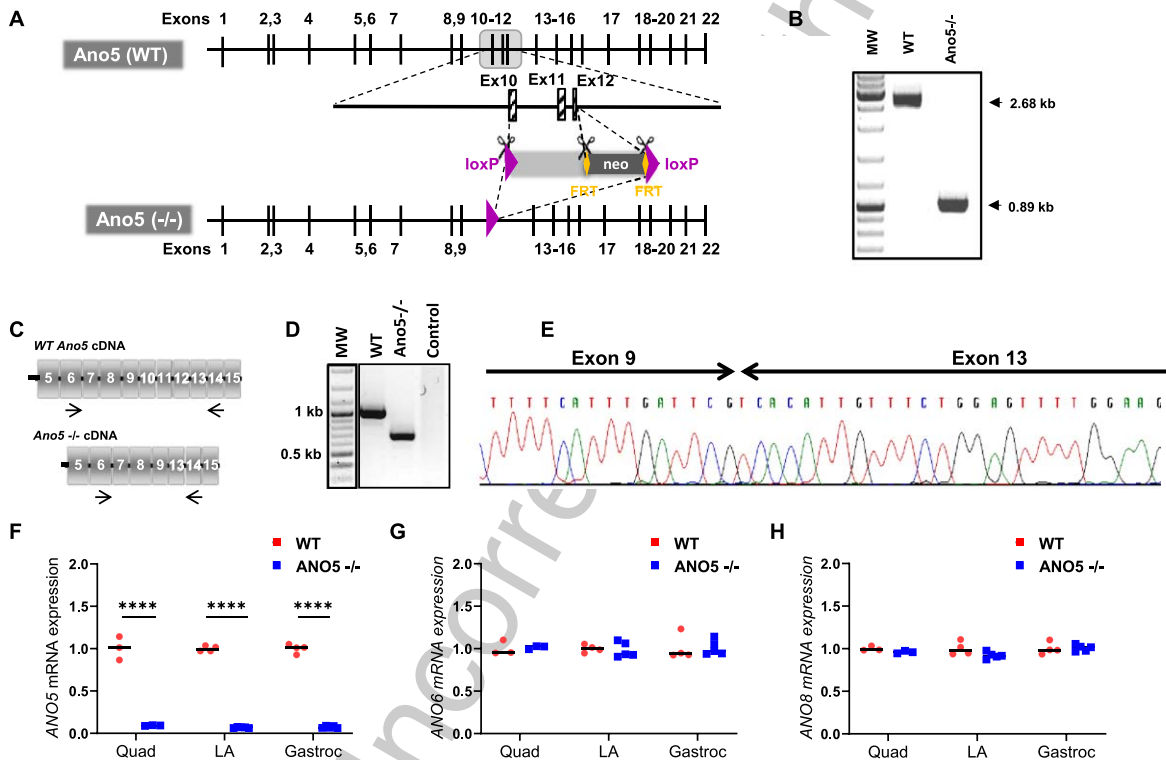


Fig. 1. Generation and genetic characterization of ANO5^{-/-} mouse model. (A) Schematic showing the genetic modifications used to disrupt the mouse *Ano5* gene in the ANO5^{-/-} mouse model. WT gene and the homologous recombination of the genome that led to the ANO5^{-/-} mice. (B) PCR analysis of the genomic region containing the deleted exonic regions shown in panel A. (C) Schematic of mRNAs resulting from WT and *Ano5*^{-/-} allele. Arrows indicate the region around which primers are designed for PCR amplification and sequencing. (D) Gel image showing PCR amplified product of the marked region of *Ano5* gene in panel C from mRNAs isolated from WT and ANO5^{-/-} mice. (E) Chromatogram showing the sequence of disrupted *Ano5* allele in the ANO5^{-/-} mouse. Plots showing qRT-PCR quantification of (F) *Ano5*, (G) *Ano6*, and (H) *Ano8*, in 9-months-old male mouse muscles (quadriceps, LA (EDL+TA), gastrocnemius). Each dot on the plot represents an individual muscle and the black bar indicates median of these values. *p* values are measured by unpaired Mann-Whitney *t* test and indicated by *****p* < 0.0001.

analysis to assess the expression of an anoctamin localized to the PM (ANO6), and one localized to the SR/PM (ANO8). Neither of these transcripts were found to be altered in their expression in the ANO5^{-/-} muscles, suggesting no compensatory change in the levels of these anoctamins in ANO5 deficient skeletal muscles (Fig. 1G, H).

Characterization of ANO5 deficient muscle

Mutations leading to loss of ANO5 protein in patients result in damage, weakness, and wasting of muscle starting from late adulthood to middle age [8, 9, 50]. Given the relative age match of middle-aged human with 9–10 month old mice, we assessed mice at this age [51]. Analysis of the body and muscle weight in ANO5^{-/-} mice compared to WT mice showed a significant drop in both body weight

and weights of multiple muscles including quadriceps, gastrocnemius, and TA (Fig. 2A–D). In view of the muscle loss induced by ANO5 deficit, we next examined if this is associated with changes in muscle histology. Cross sections of quadriceps were stained with H&E and independently immunostained to mark the basement membrane (laminin) and nuclei (DAPI) (Fig. 2E). These analyses identified the presence of a significant increase in the number of centrally nucleated myofibers in the ANO5^{-/-} muscles when compared to WT, but there were no signs of overt muscle inflammation (Fig. 2E, F). Further, the increase in regenerated (centrally nucleated) fibers occurred without any corresponding decrease in myofiber cross-sectional area of ANO5^{-/-} muscles (Fig. 2E, G). Taken together, the data suggest a lack of myofiber atrophy and/or a high rate of myofiber turnover, which would result in accumulation

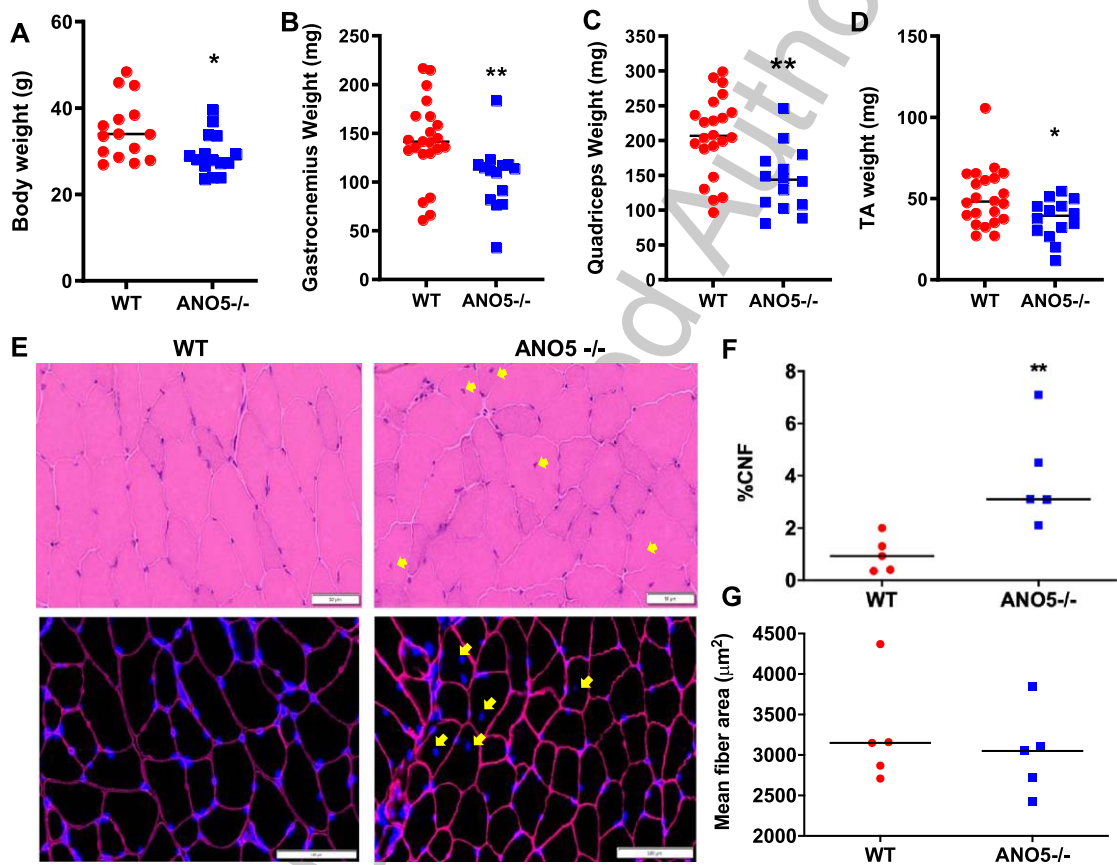


Fig. 2. Effect of ANO5 deficit on muscle size and histopathology. Plots showing (A) body weight and weights of (B) Gastrocnemius, (C) Quadriceps, and (D) TA muscles. Each dot represents an individual mouse/muscle. Images showing cross sections of quadriceps muscle (E) stained with H&E (top) and for nuclei (DAPI) and basement membrane (Laminin immunostain) (bottom). Yellow arrows mark the centrally nucleated fiber (CNF) and these were quantified to measure (F) proportion of CNFs and (G) myofiber cross-sectional areas. Each dot represents value averaged from multiple cross sections per muscle, black line represents the median value of the distribution. Scale bars are 50 μm (top) and 100 μm (bottom). *p* values are measured by unpaired Mann-Whitney *t* test and indicated by **p* < 0.05; ***p* < 0.01; A–D (*n* > 15), F, G (*n* = 5).

of small caliber regenerated myofibers. As an independent assessment of inflammation and extracellular matrix (ECM) remodeling, we performed qRT-PCR analysis to assess the expression of different regulators of inflammation, including CD3G, interleukin 1 β , interleukin 6, CD11b, and miR-142. We observed no indication for altered inflammation in the Psoas (Fig. S1A) and other ANO5 $-/-$ muscles examined (Fig. S1B). Similar analysis of the expression of ECM modulating genes – TIMP-1, Perilipin, collagen, and micro RNAs – miR-21, miR-29a, showed lack of ANO5 did not detectably alter the genes responsible for ECM remodeling in the Psoas (Figure S1C) and other muscles we examined (Figure S1D) in ANO5 $-/-$ mice.

Next, we examined the expression of multiple myogenic regulators to assess the extent of ongoing regenerative myogenesis. The expression of the myogenic indicators – embryonic myosin heavy chain (*MYH8*), myomaker (*MYMK*), embryonic myosin (*MYH3*), miR-01, and miR-31 were unaltered in the ANO5-deficient muscles (Figure S2A-C). Independently, to examine if the muscle of the 10-months old ANO5 $-/-$ mice undergo spontaneous myofiber damage and regeneration *in vivo*, we labeled spontaneously regenerating myonuclei over a 1-week period to mark all nascent myonuclei produced during this period with the nucleotide analogue BrdU delivered through the drinking water [43, 44]. As can be expected, WT mice showed no spontaneous BrdU-labeled myonuclei over this period, and we found the same is true in case of the ANO5 $-/-$ mice (Figure S2D). Thus, quantification of myogenic gene expression and spontaneous *in vivo* regenerative myogenesis in ANO5 $-/-$ mice showed a low-level spontaneous myofiber regeneration, without chronic inflammation. This is unlike the severe muscular dystrophies that are associated with extensive muscle regeneration, chronic inflammation, and excessive ECM remodeling [43, 44].

Effect of ANO5 deficit on muscle strength and sarcolemmal ion channel activity

With some of the previous ANO5 null models having reported underwhelming muscle histopathology and weakness [23, 39], we next examined muscle functional deficits in our ANO5 $-/-$ mouse model. For this we measured force production by grip strength analysis of the forelimb and hindlimb muscles of 10-month-old ANO5 $-/-$ mice. Similar to the reduced muscle strength noted in LGMD2L patients, we

found ANO5 $-/-$ mice demonstrated reduced grip strength of both the forelimb (by 4.5 KgF/Kg) and hindlimb (by 8.5 KgF/Kg), in comparison to WT controls (Fig. 3A, B). To further characterize the muscle force deficits in our ANO5 $-/-$ model, we evaluated *in vivo* muscle torque generated in response to increasing tetanic stimulations of the anterior crural muscles. Here we elicited isometric contractions by subcutaneous stimulation of the peroneal nerve across a range of frequencies from 20–200 Hz to generate a force-frequency plot. The muscles of ANO5 $-/-$ mice generated contractile force similar to the WT mice at stimulation frequencies below 80 Hz, but at tetanic stimulation frequencies (> 100 Hz) contractile force of the ANO5 $-/-$ muscle was reduced (1.2 mN-m) as compared to the WT muscle (1.6 mN-m) (Fig. 3C). These results independently demonstrate greater weakness of ANO5 $-/-$ limb muscle and reduced contractile force of these muscle during tetanic stimulation.

ANO5 protein has been suggested to operate as a plasma membrane ion channel that can be activated by a rise in intracellular Ca²⁺ [31, 34, 52]. Thus, we examined if weakness of ANO5 $-/-$ muscle is related to altered anion channel activity in the myofiber sarcolemma. For this we recorded plasma membrane currents elicited by 500 ms-duration depolarizing voltage pulses in isolated muscle fibers from WT and ANO5 $-/-$ mice in the presence of an external solution containing 149 mM or 9 mM Cl⁻ and blockers of voltage-gated Na⁺ and K⁺ channels (Fig. 3D). Depolarizations of increasing amplitudes in the presence of 149 mM Cl⁻ elicited currents displaying an early phase during which L-type voltage-gated Ca²⁺ currents activated, followed by a late phase during which voltage-gated Ca²⁺ currents inactivated and positive currents developed. These late phase positive currents were strongly reduced in the presence of 9 mM Cl⁻ in wild type and in ANO5-KO fibers indicating that the positive current recorded in the presence of the 149 mM Cl⁻ solution was mostly carried by Cl⁻ ions. In each fiber, the remaining current recorded in the presence of 9 mM Cl⁻ was subtracted from the current recorded in the presence of 149 mM Cl⁻ to extract the Cl⁻ current. The amplitude of these Cl⁻ current differences, and of the currents recorded in the presence of 149 mM Cl⁻ were measured at the end of voltage pulses in each fiber and plotted as a function of voltage. The relationships between mean current amplitudes and voltages obtained in ANO5 $-/-$ myofibers were indistinguishable from the WT myofibers (Fig. 3E). It is also noteworthy that

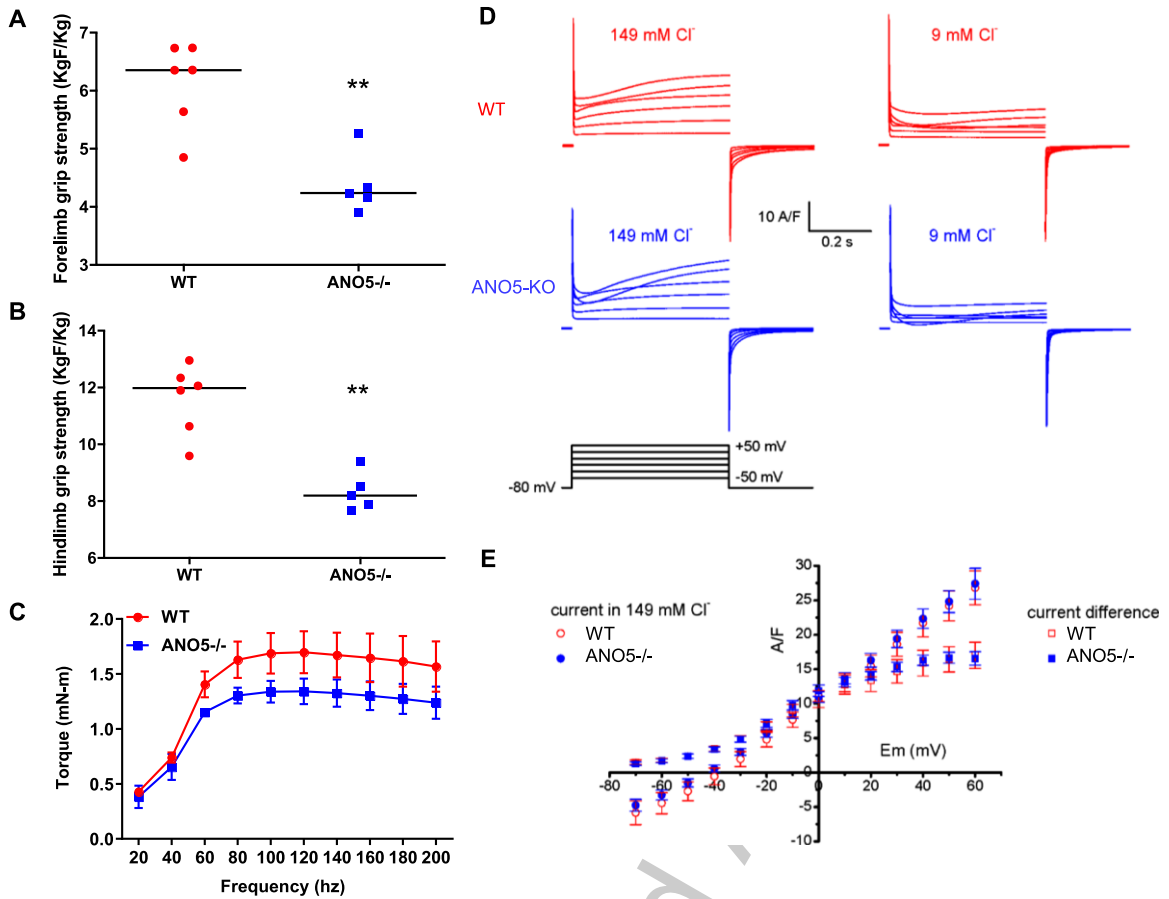


Fig. 3. Muscle strength and chloride currents in ANO5 deficient muscle. Plots for (A) hindlimb and (B) forelimb grip strength of the mice (each dot representing individual animal, black line represents the median value of the distribution.). (C) Plot showing the force-frequency relationship for the TA of mice ($n = 5$; mean \pm SD). Difference between genotypes along the frequencies was significant beyond 80Hz (Two-way ANOVA). (D) Cl⁻ currents were recorded in the same wild type (upper traces) and ANO5^{-/-} myofibers (middle traces) in the presence of either 149 mM or 9 mM external Cl⁻, in response to the voltage protocol shown in the lower traces. Voltage pulses were delivered every 5 s. (E) Relationships between the voltage and the mean end-pulse amplitude of the current measured in the presence of 149 mM Cl⁻ and of the current difference (current in 149 mM Cl⁻ minus current in 9 mM Cl⁻) in 12 fibers from wild type and in 13 fibers from two ANO5-KO mice. p values are measured by unpaired Mann-Whitney t test (A, B) or 2-way ANOVA (C) and indicated by ** $p < 0.01$, $n \geq 5$.

all fibers we tested contracted in response to voltage pulses given above -30 mV, allowing us to exclude the possibility that ANO5 did not activate due to absence of intracellular Ca²⁺ rise. Lack of detectable difference in depolarization evoked Cl⁻ currents on myofiber sarcolemma between WT and ANO5^{-/-} myofibers indicates that ANO5 does not function as a sarcolemmal Cl⁻ channel in muscle fibers and that weakness of ANO5^{-/-} myofibers cannot be attributed to altered sarcolemmal Cl⁻ channel activity.

In vivo role of ANO5 on muscle regeneration

The ability to regulate myoblast fusion is another role attributed to ANO5 [34, 37]. In previous analysis of ANO5 deficient patient myoblasts we did not

observe a myogenic deficit *in vitro* [35]. With the availability of the ANO5^{-/-} model, we next examined the role of ANO5 in regenerative myogenesis *in vivo*. For this we used BrdU-labeling of activated myogenic cells to monitor spontaneous regenerative myogenesis [43, 44]. We used this approach in combination with notexin-based, sterile injury to investigate myogenic cell fusion after synchronized muscle damage [42, 53]. Here, the quantification of BrdU-labeled central nuclei in recently regenerated myofibers provides a readout of satellite cell activation and myogenic cell fusion in response to *in vivo* muscle injury. Following injury, BrdU was administered to the WT and the ANO5^{-/-} mice for 7- or 14-days and the muscle cross-sections were scored for presence of BrdU stained central-myonuclei to

502
503
504
505
506
507
508
509
510
511
512
513
514
515

516
517
518
519
520
521
522
523
524
525
526
527
528
529
530
531

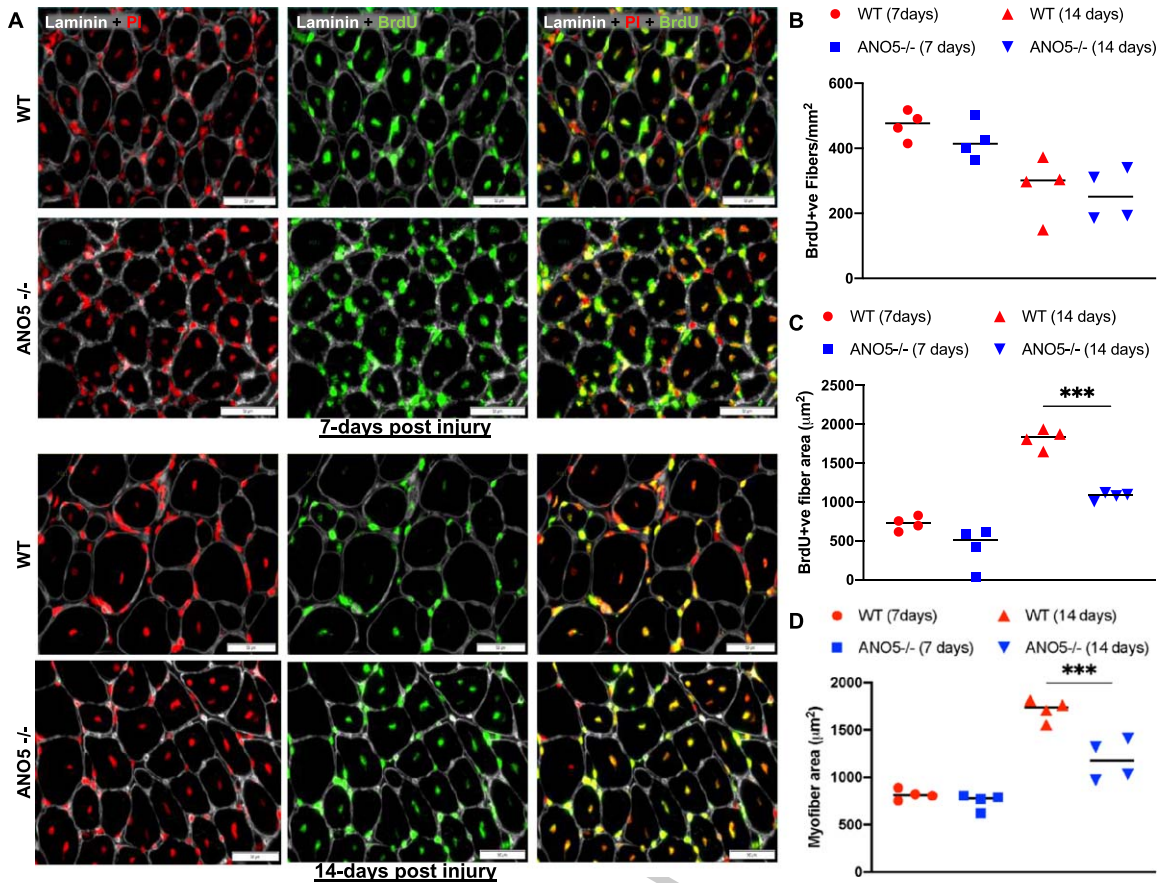


Fig. 4. Analysis of regenerative myogenesis *in vivo*. (A) Images of NTX-injured TA muscle cross-sections stained for regenerated myonuclei (BrdU), nuclei (propidium iodide – PI) and basement membrane (Laminin) from WT and ANO5^{-/-} mice at 7 days (upper panel) or 14 days (lower panel) post single bout of injury. (B) Plot showing number of myofibers in individual muscle cross section that contained BrdU-labeled myonuclei (C, D) Plot showing mean fiber cross-sectional area for (C) myofibers containing BrdU-labeled nuclei. (D) all myofibers in the muscle cross-section. Scale bar - 100 µm. Data represents mean ± SD with each dot representing value from whole muscle cross-section from individual mouse muscle. *p* values are measured by two-way ANOVA with Tukey's multiple comparisons test and indicated by ***p* < 0.01, ****p* < 0.001, *n* = 4.

532 identify the newly regenerated myofibers, while
 533 all nuclei were stained with propidium iodide and
 534 myofiber boundary was marked with laminin stain-
 535 ing (Fig. 4A). Both WT and ANO5^{-/-} muscle showed
 536 abundant BrdU labeled myofibers at 7-days and at
 537 14-days post injury (Fig. 4A). Quantification of the
 538 number of BrdU-labeled myofibers identified no differ-
 539 ence between the WT and ANO5^{-/-} muscles at
 540 either 7-days or 14-days post injury (Fig. 4B). This
 541 indicated no detectable deficit in regenerative myo-
 542 genesis on account of *in vivo* myoblast fusion deficit
 543 in ANO5^{-/-} mouse muscle. Previous studies identi-
 544 fied that the size of the newly regenerated myofibers
 545 was reduced at 30 days or 90 days post myotoxin
 546 injury [37]. We thus measured growth of newly
 547 regenerated myofibers at 7- and 14-days post injury.
 548 While average myofiber size at 7-days post injury

549 was not different between the WT and ANO5^{-/-}
 550 mouse muscles, the average size of freshly regen-
 551 erated (BrdU-labeled) ANO5^{-/-} fibers was lower at
 552 14-days post injury relative to control (Fig. 4C). This
 553 difference was significant even when fibers that did
 554 not contain a BrdU labeled nuclei were also included
 555 in the quantification of the myofiber cross-sectional
 556 area (Fig. 4D). These findings indicate that while the
 557 lack of ANO5 does not compromise myoblast fusion
 558 *in vivo*, it slows subsequent myofiber growth.

559 DISCUSSION

560 With the increasing identification of LGM
 561 D2L/R12 muscular dystrophy patients [54–56], there
 562 is a growing need to develop suitable animal mod-
 563 els to help understand the *in vivo* role of ANO5

564 protein and test therapies which target this deficit.
565 Our study has generated such a mouse model that
566 mimics several clinical features of ANO5 deficit
567 in LGMD2L/R12 ranging from muscle weakness,
568 myofiber damage, and progressive muscle loss. We
569 created this model by the deletion of exons 10–12
570 of mouse *Ano5* gene, which selectively prevented the
571 expression of this gene without affecting the expres-
572 sion of the other anoctamin family members tested.
573 This is different from a previous ANO5 mouse model
574 with a reading frameshift caused by exon 11–12 dele-
575 tion that results in the loss of *Ano5* transcript in bone
576 and 71% reduction in muscle, leading to GDD-like
577 bone defects [40]. Our observation of muscle pathol-
578 ogy caused by the deletion of exons 10–12 aligns with
579 muscle pathology caused by the deletion of exons 8–9
580 in the mouse, and of exons 12–13 in the rabbit, but
581 not in mice where exons 1, 2 are deleted [23, 37, 39,
582 41].

583 The mouse model we describe shows reduced
584 total body mass and reduced muscle mass, recapit-
585 ulating the muscle wasting and loss reported in the
586 human patients [6, 8, 57]. These ANO5-deficient
587 mouse muscles also showed reduced muscle strength
588 reported in the patients [6, 8]. In addition to the
589 reduced forelimb and hindlimb grip strength in
590 ANO5^{-/-} mice, the TA muscle of these mice also
591 fatigue faster and show reduced isometric force at
592 tetanic stimulation as compared to the WT mice. This
593 latter response of ANO5^{-/-} muscle is in addition
594 to our recent observation that lengthening contrac-
595 tion (LC) of the EDL muscle leads to greater muscle
596 force drop in the ANO5^{-/-} muscle as compared to
597 WT muscle [24]. Poor recovery of ANO5^{-/-} mus-
598 cle from LC injury occurs due to impaired ability
599 of these myofibers to undergo sarcolemmal repair
600 – a deficit documented in patient muscle cells and
601 another ANO5-deficient mouse model [24, 35, 37,
602 38]. Poor sarcolemmal repair caused by ANO5 deficit
603 could also contribute to muscle loss and to muscle
604 weakness observed here in the ANO5^{-/-} mice.

605 Impaired myofiber sarcolemmal repair in the
606 LGMD2L/R12 mouse model is shared with the
607 LGMD2B/R2 mouse model, where mutations affect
608 the dysferlin protein [27, 58]. Similar to dysferlin,
609 ANO5 protein also translocate to the injured plasma
610 membrane in myoblasts and in mature myofibers [27,
611 35, 38, 59]. However, unlike the LGMD2B patients
612 and mice, which show adipogenic muscle loss [42,
613 57], we did not observe this as a feature of ANO5^{-/-}
614 muscle. This suggests that dysferlin and ANO5 pro-
615 tein have different functions leading to different

616 manifestation of disease symptoms. In support of this,
617 our previous work has shown that AAV-based expres-
618 sion of ANO5 in dysferlin-deficient mouse muscle
619 fails to rescue the sarcolemmal repair and other symp-
620 toms of the dysferlin-deficient mouse [60]. Indeed,
621 ANO5 and dysferlin have distinct roles in sarcolem-
622 mal repair. While dysferlin regulates membrane
623 repair through regulation of lysosome fusion, loss of
624 ANO5 compromises handling of cytosolic Ca²⁺ and
625 impairs membrane repair mediated by annexin, mito-
626 chondrial signaling, and phosphatidylserine lipids
627 [24, 35–38]. Dysferlin deficit alters the homeostasis
628 of another membrane lipid – sphingomyelin, and use
629 of the sphingomyelinase enzyme as well as improving
630 the stability of the dysferlinopathic myofiber mem-
631 brane improves repair and reduces muscle loss [45,
632 58]. Aside from membrane lipid alteration, dysferlin-
633 and ANO5-deficient muscles also show cellular Ca²⁺
634 dysregulation upon myofiber stress/damage [24, 61,
635 62].

636 The above role of ANO5 in SR Ca²⁺ homeos-
637 tasis is due to its ability to function as an anion
638 channel at the ER membrane [24]. Cellular mod-
639 els with exogenous ANO5 overexpression leading
640 to the presence of ANO5 at the plasma membrane
641 enables Ca²⁺-activated ion channel activity [30, 31,
642 63]. However, our analysis of the chloride channel
643 activity at the plasma membrane of ANO5-deficient
644 mouse myofibers showed no difference in this activity
645 between ANO5^{-/-} and WT myofibers. This could be
646 either due to the lack of anion channel activity of the
647 plasma membrane-localized ANO5, or that endoge-
648 nous ANO5 protein shows little (or no) expression
649 at the plasma membrane, resulting in no detectable
650 channel activity at the sarcolemma. Indeed, ANO5
651 localizes at the ER membrane and alters ER ion
652 homeostasis when absent [24, 26, 35]. Aside from ion
653 channel activity, ANO5 also possesses lipid scram-
654 blase activity, which has been implicated in regulation
655 of myoblast fusion *in vitro* [34, 37]. Our *in vivo*
656 analysis shows no significant spontaneous regener-
657 ative myogenesis in the adult ANO5^{-/-} muscle and
658 no difference in the ability of the satellite cells in
659 the injured muscle to undergo fusion to regener-
660 ate the lost myofibers, which is in agreement with
661 the *in vitro* studies using patient-derived myoblasts
662 [35]. Interestingly, we observed that growth of the
663 freshly regenerated ANO5^{-/-} myofibers is slower as
664 compared to the matched WT myofibers, recapitulat-
665 ing a similar observation in another ANO5-deficient
666 mouse model [37]. Thus, while ANO5 deficit in
667 mouse myoblast was found to impair their myogenic

fusion *in vitro*, this role of ANO5 does not extend *in vivo* in mouse muscle nor to *in vitro* patient cell fusion. Additional studies will be needed to extend this analysis to other patient mutations and to determine the basis of such *in vivo* versus *in vitro* differences. Lack of myogenic fusion deficit in human myoblasts *in vitro*, and in mouse myofibers *in vivo* indicate that poor myogenesis may not be the basis for muscle loss in the LGMD2L/R12 patients, but the slower growth of nascent regenerated myofibers could contribute to the muscle weakness.

In summary, the findings we report in this study establishes a new mouse model for LGMD2L/R12 that manifests multiple muscle pathologies reported in ANO5 deficient muscular dystrophy patients. Description of these muscle pathologies and physiological deficits reported here and our earlier studies identifying a therapeutic approach to improve repair of ANO5^{-/-} myofibers demonstrate the utility of this model to improve our understanding of the mechanisms of ANO5 function in skeletal muscle and testing therapies to treat muscular dystrophy caused by its deficit.

ACKNOWLEDGMENTS

This study was supported by funds from Association Française contre les Myopathies (AFM) to IR. JKJ acknowledges financial support from the National Institute of Health grants (R01AR055686, R21HD103993, P50HD105328), and thanks Dr. Terry Partridge for his insights into myogenesis, studying its role using mouse models of diseases, and the use of BrdU-labeling approach employed in this study. IR and JKJ conceived this study, obtained funds for this study and supervised the work. GT and SSC conducted all the functional studies with help from GC, JN, and MH for muscle exercise and myogenesis analysis. IR, KC, LS-P generated the knockout mouse and conducted its molecular characterization. BA conducted and described the electrophysiological analysis. GT and JKJ wrote the manuscript with help from IR and all the other authors.

CONFLICT OF INTEREST

Authors declare no conflict of interests.

REFERENCES

- [1] Bushby K. Diagnostic criteria for the limb-girdle muscular dystrophies: report of the ENMC consortium on

limbgirdle dystrophies. *Neuromuscular Disorders*. 1995; 5(1):71-4.

- [2] Angelini C. LGMD. Identification, description and classification. *Acta Myol*. 2020;39(4):207-17.
- [3] Georganopoulou DG, Moisiadis VG, Malik FA, Mohajer A, Dashevsky TM, Wu ST, et al. A Journey with LGMD: From Protein Abnormalities to Patient Impact. *Protein J*. 2021;40(4):466-88.
- [4] Ten Dam L, Frankhuizen WS, Linssen W, Straathof CS, Niks EH, Faber K, et al. Autosomal recessive limb-girdle and Miyoshi muscular dystrophies in the Netherlands: The clinical and molecular spectrum of 244 patients. *Clin Genet*. 2019;96(2):126-33.
- [5] Nallamilli BRR, Chakravorty S, Kesari A, Tanner A, Ankala A, Schneider T, et al. Genetic landscape and novel disease mechanisms from a large LGMD cohort of 4656 patients. *Ann Clin Transl Neurol*. 2018;5(12):1574-87.
- [6] Bolduc V, Marlow G, Boycott KM, Saleki K, Inoue H, Kroon J, et al. Recessive mutations in the putative calcium-activated chloride channel Anoctamin 5 cause proximal LGMD2L and distal MMD3 muscular dystrophies. *American journal of human genetics*. 2010;86(2):213-21.
- [7] Sarkozy A, Hicks D, Hudson J, Laval SH, Barresi R, Hilton-Jones D, et al. ANO5 gene analysis in a large cohort of patients with anoctaminopathy: confirmation of male prevalence and high occurrence of the common exon 5 gene mutation. *Human mutation*. 2013;34(8):1111-8.
- [8] Hicks D, Sarkozy A, Muelas N, Koehler K, Huebner A, Hudson G, et al. A founder mutation in Anoctamin 5 is a major cause of limb-girdle muscular dystrophy. *Brain : a journal of neurology*. 2011;134(Pt 1):171-82.
- [9] Mahjneh I, Jaiswal J, Lamminen A, Somer M, Marlow G, Kiuru-Enari S, et al. A new distal myopathy with mutation in anoctamin 5. *Neuromuscular disorders: NMD*. 2010;20(12):791-5.
- [10] Whitlock JM, Hartzell HC. Anoctamins/TMEM16 Proteins: Chloride Channels Flirting with Lipids and Extracellular Vesicles. *Annu Rev Physiol*. 2017;79:119-43.
- [11] Boccaccio A, Di Zanni E, Gradogna A, Scholz-Starke J. Lifting the veils on TMEM16E function. *Channels*. 2019;13(1):33-5.
- [12] Tian Y, Schreiber R, Kunzelmann K. Anoctamins are a family of Ca²⁺-activated Cl⁻ channels. *Journal of cell science*. 2012;125(Pt 21):4991-8.
- [13] Berg J, Yang H, Jan LY. Ca²⁺-activated Cl⁻ channels at a glance. *Journal of cell science*. 2012;125(6):1367-71.
- [14] Yang YD, Cho H, Koo JY, Tak MH, Cho Y, Shim W-S, et al. TMEM16A confers receptor-activated calcium-dependent chloride conductance. *Nature*. 2008;455(7217):1210-5.
- [15] Schroeder BC, Cheng T, Jan YN, Jan LY. Expression cloning of TMEM16A as a calcium-activated chloride channel subunit. *Cell*. 2008;134(6):1019-29.
- [16] Caputo A, Caci E, Ferrera L, Pedemonte N, Barsanti C, Sondo E, et al. TMEM16A, a membrane protein associated with calcium-dependent chloride channel activity. *Science*. 2008;322(5901):590-4.
- [17] Pifferi S, Dibattista M, Menini A. TMEM16B induces chloride currents activated by calcium in mammalian cells. *Pflügers Archiv : European journal of physiology*. 2009;458(6):1023-38.
- [18] Stohr H, Heisig JB, Benz PM, Schoberl S, Milenkovic VM, Strauss O, et al. TMEM16B, a novel protein with calcium-dependent chloride channel activity, associates with a presynaptic protein complex in photoreceptor terminals. *J Neurosci*. 2009;29(21):6809-18.

- 779 [19] Tsuji T, Cheng J, Tatematsu T, Ebata A, Kamikawa H, Fujita A, et al. Predominant localization of phosphatidylserine at the cytoplasmic leaflet of the ER, and its TMEM16K-dependent redistribution. Proceedings of the National Academy of Sciences. 2019;116(27):13368-73. 780 781 782 783 784
- [20] Petkovic M, Oses-Prieto J, Burlingame A, Jan LY, Jan YN. TMEM16K is an interorganelle regulator of endosomal sorting. Nature communications. 2020;11(1):1-16. 785 786 787
- [21] Suzuki J, Fujii T, Imao T, Ishihara K, Kuba H, Nagata S. Calcium-dependent phospholipid scramblase activity of TMEM16 protein family members. The Journal of biological chemistry. 2013;288(19):13305-16. 788 789 790 791
- [22] Alvadia C, Lim NK, Mosina VC, Oostergetel GT, Dutzler R, Paulino C. Cryo-EM structures and functional characterization of the murine lipid scramblase TMEM16F. Elife. 2019;8:e44365. 792 793 794 795
- [23] Xu J, El Refaey M, Xu L, Zhao L, Gao Y, Floyd K, et al. Genetic disruption of Ano5 in mice does not recapitulate human ANO5-deficient muscular dystrophy. Skelet Muscle. 2015;5:43. 796 797 798 799
- [24] Chandra G, Sreetama SC, Mázala DA, Charton K, VanderMeulen JH, Richard I, et al. Endoplasmic reticulum maintains ion homeostasis required for plasma membrane repair. Journal of Cell Biology. 2021;220(5). 800 801 802 803
- [25] Mizuta K, Tsutsumi S, Inoue H, Sakamoto Y, Miyatake K, Miyawaki K, et al. Molecular characterization of GDD1/TMEM16E, the gene product responsible for autosomal dominant gnathodiaphyseal dysplasia. Biochemical and biophysical research communications. 2007;357(1):126-32. 804 805 806 807 808 809
- [26] Tsutsumi S, Kamata N, Vokes TJ, Maruoka Y, Nakakuki K, Enomoto S, et al. The novel gene encoding a putative transmembrane protein is mutated in gnathodiaphyseal dysplasia (GDD). American journal of human genetics. 2004;74(6):1255-61. 810 811 812 813 814
- [27] Bansal D, Miyake K, Vogel SS, Groh S, Chen CC, Williamson R, et al. Defective membrane repair in dysferlin-deficient muscular dystrophy. Nature. 2003;423(6936):168-72. 815 816 817 818 819
- [28] Ho M, Post CM, Donahue LR, Lidov HG, Bronson RT, Goolsby H, et al. Disruption of muscle membrane and phenotype divergence in two novel mouse models of dysferlin deficiency. Hum Mol Genet. 2004;13(18):1999-2010. 820 821 822 823 824
- [29] Liu J, Aoki M, Illa I, Wu C, Fardeau M, Angelini C, et al. Dysferlin, a novel skeletal muscle gene, is mutated in Miyoshi myopathy and limb girdle muscular dystrophy. Nat Genet. 1998;20(1):31-6. 825 826 827 828 829 830
- [30] Di Zanni E, Gradogna A, Picco C, Scholz-Starke J, Boccaccio A. TMEM16E/ANO5 mutations related to bone dysplasia or muscular dystrophy cause opposite effects on lipid scrambling. Human mutation. 2020;41(6):1157-70. 831 832 833 834 835 836
- [31] Di Zanni E, Gradogna A, Scholz-Starke J, Boccaccio A. Gain of function of TMEM16E/ANO5 scrambling activity caused by a mutation associated with gnathodiaphyseal dysplasia. Cellular and molecular life sciences: CMLS. 2018;75(9):1657-70. 837 838 839 840 841 842
- [32] Gyobu S, Ishihara K, Suzuki J, Segawa K, Nagata S. Characterization of the scrambling domain of the TMEM16 family. Proc Natl Acad Sci U S A. 2017;114(24):6274-9. 900 901 902 903
- [33] Duran C, Qu Z, Osunkoya AO, Cui Y, Hartzell HC. ANO5 3-7 in the anoctamin/Tmem16 Cl- channel family are intracellular proteins. American journal of physiology Cell physiology. 2012;302(3):C482-93. 904 905 906
- [34] Whitlock JM, Yu K, Cui YY, Hartzell HC. Anoctamin 5/TMEM16E facilitates muscle precursor cell fusion. J Gen Physiol. 2018;150(11):1498-509. 843 844 845 846 847 848 849 850 851 852 853 854 855 856 857 858 859 860 861 862 863 864 865 866 867 868 869 870 871 872 873 874 875 876 877 878 879 880 881 882 883 884 885 886 887 888 889 890 891 892 893 894 895 896 897 898 899 900 901 902 903 904 905 906
- [35] Chandra G, Defour A, Mamchoui K, Pandey K, Mishra S, Mouly V, et al. Dysregulated calcium homeostasis prevents plasma membrane repair in Anoctamin 5/TMEM16E-deficient patient muscle cells. Cell death discovery. 2019;5(1):1-15. 846 847 848 849 850 851 852 853 854 855 856 857 858 859 860 861 862 863 864 865 866 867 868 869 870 871 872 873 874 875 876 877 878 879 880 881 882 883 884 885 886 887 888 889 890 891 892 893 894 895 896 897 898 899 900 901 902 903 904 905 906
- [36] Jaiswal JK, Marlow G, Summerill G, Mahjneh I, Mueller S, Hill M, et al. Patients with a non-dysferlin Miyoshi myopathy have a novel membrane repair defect. Traffic. 2007;8(1):77-88. 846 847 848 849 850 851 852 853 854 855 856 857 858 859 860 861 862 863 864 865 866 867 868 869 870 871 872 873 874 875 876 877 878 879 880 881 882 883 884 885 886 887 888 889 890 891 892 893 894 895 896 897 898 899 900 901 902 903 904 905 906
- [37] Griffin DA, Johnson RW, Whitlock JM, Pozsgai ER, Heller KN, Grose WE, et al. Defective membrane fusion and repair in Anoctamin5-deficient muscular dystrophy. Human molecular genetics. 2016;25(10):1900-11. 846 847 848 849 850 851 852 853 854 855 856 857 858 859 860 861 862 863 864 865 866 867 868 869 870 871 872 873 874 875 876 877 878 879 880 881 882 883 884 885 886 887 888 889 890 891 892 893 894 895 896 897 898 899 900 901 902 903 904 905 906
- [38] Foltz SJ, Cui YY, Choo HJ, Hartzell H. ANO5 ensures trafficking of annexins in wounded myofibers. Journal of Cell Biology. 2021;220(3). 846 847 848 849 850 851 852 853 854 855 856 857 858 859 860 861 862 863 864 865 866 867 868 869 870 871 872 873 874 875 876 877 878 879 880 881 882 883 884 885 886 887 888 889 890 891 892 893 894 895 896 897 898 899 900 901 902 903 904 905 906
- [39] Gyobu S, Miyata H, Ikawa M, Yamazaki D, Takeshima H, Suzuki J, et al. A Role of TMEM16E Carrying a Scrambling Domain in Sperm Motility. Molecular and cellular biology. 2016;36(4):645-59. 846 847 848 849 850 851 852 853 854 855 856 857 858 859 860 861 862 863 864 865 866 867 868 869 870 871 872 873 874 875 876 877 878 879 880 881 882 883 884 885 886 887 888 889 890 891 892 893 894 895 896 897 898 899 900 901 902 903 904 905 906
- [40] Wang X, Liu X, Dong R, Liang C, Reichenberger EJ, Hu Y. Genetic disruption of anoctamin 5 in mice replicates human gnathodiaphyseal dysplasia (GDD). Calcified tissue international. 2019;104(6):679-89. 846 847 848 849 850 851 852 853 854 855 856 857 858 859 860 861 862 863 864 865 866 867 868 869 870 871 872 873 874 875 876 877 878 879 880 881 882 883 884 885 886 887 888 889 890 891 892 893 894 895 896 897 898 899 900 901 902 903 904 905 906
- [41] Sui T, Xu L, Lau YS, Liu D, Liu T, Gao Y, et al. Development of muscular dystrophy in a CRISPR-engineered mutant rabbit model with frame-disrupting ANO5 mutations. Cell Death Dis. 2018;9(6):609. 846 847 848 849 850 851 852 853 854 855 856 857 858 859 860 861 862 863 864 865 866 867 868 869 870 871 872 873 874 875 876 877 878 879 880 881 882 883 884 885 886 887 888 889 890 891 892 893 894 895 896 897 898 899 900 901 902 903 904 905 906
- [42] Hogarth MW, Defour A, Lazarski C, Gallardo E, Diaz Manera J, Partridge TA, et al. Fibroadipogenic progenitors are responsible for muscle loss in limb girdle muscular dystrophy 2B. Nat Commun. 2019;10(1):2430. 846 847 848 849 850 851 852 853 854 855 856 857 858 859 860 861 862 863 864 865 866 867 868 869 870 871 872 873 874 875 876 877 878 879 880 881 882 883 884 885 886 887 888 889 890 891 892 893 894 895 896 897 898 899 900 901 902 903 904 905 906
- [43] Mazala DA, Novak JS, Hogarth MW, Nearing M, Adusumalli P, Tully CB, et al. TGF-beta-driven muscle degeneration and failed regeneration underlie disease onset in a DMD mouse model. JCI Insight. 2020;5(6). 846 847 848 849 850 851 852 853 854 855 856 857 858 859 860 861 862 863 864 865 866 867 868 869 870 871 872 873 874 875 876 877 878 879 880 881 882 883 884 885 886 887 888 889 890 891 892 893 894 895 896 897 898 899 900 901 902 903 904 905 906
- [44] Novak JS, Hogarth MW, Boehler JF, Nearing M, Vila MC, Heredia R, et al. Myoblasts and macrophages are required for therapeutic morpholino antisense oligonucleotide delivery to dystrophic muscle. Nat Commun. 2017;8(1):941. 846 847 848 849 850 851 852 853 854 855 856 857 858 859 860 861 862 863 864 865 866 867 868 869 870 871 872 873 874 875 876 877 878 879 880 881 882 883 884 885 886 887 888 889 890 891 892 893 894 895 896 897 898 899 900 901 902 903 904 905 906
- [45] Sreetama SC, Chandra G, Van der Meulen JH, Ahmad MM, Suzuki P, Bhuvanendran S, et al. Membrane Stabilization by Modified Steroid Offers a Potential Therapy for Muscular Dystrophy Due to Dysferlin Deficit. Mol Ther. 2018;26(9):2231-42. 846 847 848 849 850 851 852 853 854 855 856 857 858 859 860 861 862 863 864 865 866 867 868 869 870 871 872 873 874 875 876 877 878 879 880 881 882 883 884 885 886 887 888 889 890 891 892 893 894 895 896 897 898 899 900 901 902 903 904 905 906
- [46] Bittel AJ, Sreetama SC, Bittel DC, Horn A, Novak JS, Yokota T, et al. Membrane Repair Deficit in Facioscapulothoracic Muscular Dystrophy. Int J Mol Sci. 2020;21(15). 846 847 848 849 850 851 852 853 854 855 856 857 858 859 860 861 862 863 864 865 866 867 868 869 870 871 872 873 874 875 876 877 878 879 880 881 882 883 884 885 886 887 888 889 890 891 892 893 894 895 896 897 898 899 900 901 902 903 904 905 906
- [47] Idoux R, Fuster C, Jacquemond V, Dayal A, Grabner M, Charnet P, et al. Divalent cations permeation in a Ca(2+) non-conducting skeletal muscle dihydropyridine receptor mouse model. Cell Calcium. 2020;91:102256. 846 847 848 849 850 851 852 853 854 855 856 857 858 859 860 861 862 863 864 865 866 867 868 869 870 871 872 873 874 875 876 877 878 879 880 881 882 883 884 885 886 887 888 889 890 891 892 893 894 895 896 897 898 899 900 901 902 903 904 905 906
- [48] Jha A, Chung WY, Vachel L, Maleth J, Lake S, Zhang G, et al. Anoctamin 8 tethers endoplasmic reticulum and plasma membrane for assembly of Ca2+signaling complexes at the ER/PM compartment. The EMBO journal. 2019;38(12):e101452. 846 847 848 849 850 851 852 853 854 855 856 857 858 859 860 861 862 863 864 865 866 867 868 869 870 871 872 873 874 875 876 877 878 879 880 881 882 883 884 885 886 887 888 889 890 891 892 893 894 895 896 897 898 899 900 901 902 903 904 905 906
- [49] Wu N, Cernysiov V, Davidson D, Song H, Tang J, Luo S, et al. Critical role of lipid scramblase TMEM16F in phosphatidylserine exposure and repair of plasma membrane after pore formation. Cell reports. 2020;30(4):1129-40. e5. 846 847 848 849 850 851 852 853 854 855 856 857 858 859 860 861 862 863 864 865 866 867 868 869 870 871 872 873 874 875 876 877 878 879 880 881 882 883 884 885 886 887 888 889 890 891 892 893 894 895 896 897 898 899 900 901 902 903 904 905 906

- 907 [50] Witting N, Duno M, Petri H, Krag T, Bundgaard H, Kober L, et al. Anoctamin 5 muscular dystrophy in
908 Denmark: prevalence, genotypes, phenotypes, cardiac find-
909 ings, and muscle protein expression. *Journal of neurology*.
910 2013;260(8):2084-93.
- 911 [51] Rae EA, Brown RE. The problem of genotype and sex dif-
912 ferences in life expectancy in transgenic AD mice. *Neurosci*
913 *Biobehav Rev*. 2015;57:238-51.
- 914 [52] Tran TT, Tobiume K, Hirono C, Fujimoto S, Mizuta K,
915 Kubozono K, et al. TMEM16E (GDD1) exhibits protein
916 instability and distinct characteristics in chloride chan-
917 nel/pore forming ability. *Journal of cellular physiology*.
918 2014;229(2):181-90.
- 919 [53] Leikina E, Defour A, Melikov K, Van der Meulen JH,
920 Nagaraju K, Bhuvanendran S, et al. Annexin A1 deficiency
921 does not affect myofiber repair but delays regeneration of
922 injured muscles. *Scientific reports*. 2015;5(1):1-12.
- 923 [54] Savarese M, Di Fruscio G, Tasca G, Ruggiero L, Janssens S,
924 De Bleecker J, et al. Next generation sequencing on patients
925 with LGMD and nonspecific myopathies: Findings asso-
926 ciated with ANO5 mutations. *Neuromuscular disorders*:
927 *NMD*. 2015;25(7):533-41.
- 928 [55] Kuhn M, Glaser D, Joshi PR, Zierz S, Wenninger S, Schoser
929 B, et al. Utility of a next-generation sequencing-based gene
930 panel investigation in German patients with genetically
931 unclassified limb-girdle muscular dystrophy. *Journal of neu-*
932 *rology*. 2016;263(4):743-50.
- 933 [56] Bohlega S, Monies DM, Abulaban AA, Murad HN, Alhindi
934 HN, Meyer BF. Clinical and genetic features of anoc-
935 taminopathy in Saudi Arabia. *Neurosciences (Riyadh)*.
936 2015;20(2):173-7.
- 937 [57] Ten Dam L, van der Kooij AJ, Rovekamp F, Linssen WH,
938 de Visser M. Comparing clinical data and muscle imaging
939 of DYSF and ANO5 related muscular dystrophies. *Neuro-*
940 *muscular disorders: NMD*. 2014;24(12):1097-102.
- 941 [58] Defour A, Van der Meulen JH, Bhat R, Bigot A, Bashir
942 R, Nagaraju K, et al. Dysferlin regulates cell membrane
943 repair by facilitating injury-triggered acid sphingomyeli-
944 nase secretion. *Cell Death Dis*. 2014;5:e1306.
- 945 [59] Bittel DC, Chandra G, Tirunagri LMS, Deora AB, Medikay-
946 ala S, Scheffer L, et al. Annexin A2 Mediates Dysferlin
947 Accumulation and Muscle Cell Membrane Repair. *Cells*.
948 2020;9(9).
- 949 [60] Monjaret F, Suel-Petat L, Bourg-Alibert N, Vihola A,
950 Marchand S, Roudaut C, et al. The phenotype of
951 dysferlin-deficient mice is not rescued by adeno-associated
952 virus-mediated transfer of anoctamin 5. *Human gene ther-*
953 *apy Clinical development*. 2013;24(2):65-76.
- 954 [61] Kerr JP, Ziman AP, Mueller AL, Muriel JM, Kleinhans-
955 Welte E, Gumerson JD, et al. Dysferlin stabilizes stress-
956 induced Ca²⁺-signaling in the transverse tubule membrane.
957 *Proc Natl Acad Sci U S A*. 2013;110(51):20831-6.
- 958 [62] Chandra G, Mazala DAG, Jaiswal JK. Coping with the cal-
959 cium overload caused by cell injury: ER to the rescue. *Cell*
960 *Stress*. 2021;5(5):73-5.
- 961 [63] Schreiber R, Ousingasawat J, Kunzelmann K. Targeting of
962 Intracellular TMEM16 Proteins to the Plasma Membrane
963 and Activation by Purinergic Signaling. *International jour-*
964 *nal of molecular sciences*. 2020;21(11):4065.
- 965